Elucidating transient macromolecular interactions using paramagnetic relaxation enhancement

G Marius Clore, Chun Tang and Junji Iwahara[*]

Recent advances in the use of paramagnetic relaxation enhancement (PRE) in structure refinement and in the analysis of transient dynamic processes involved in macromolecular complex formation are presented. In the slow exchange regime, we show, using the SRY/DNA complex as an example, that the PRE provides a powerful tool that can lead to significant increases in the reliability and accuracy of NMR structure determinations. Refinement necessitates the use of an ensemble representation of the paramagnetic center and a model-free extension of the Solomon–Bloembergen equations. In the fast exchange regime, the PRE provides insight into dynamic processes and the existence of transient, low population intermediate species. The PRE allows one to characterize dynamic nonspecific binding of a protein to DNA; to directly demonstrate that the search process whereby a transcription factor locates its specific DNA target site involves both intramolecular (sliding) and intermolecular (hopping and intersegment transfer) translocation; and to detect and visualize the distribution of an ensemble of transient encounter complexes in protein–protein association.

Addresses
Laboratory of Chemical Physics, Building 5, National Institute of Diabetes and Digestive and Kidney Diseases, National Institutes of Health, Bethesda, MD 20892-0520, USA

Corresponding author: Clore, G Marius (mariusc@intra.niddk.nih.gov)
[*] Present address: Sealy Center for Structural Biology, University of Texas Medical Branch, 301 University Boulevard, Galveston, TX 775555-1068, USA.

Abbreviations

NMR	nuclear magnetic resonance
PRE	paramagnetic relaxation enhancement
NOE	nuclear Overhauser effect
HSQC	heteronuclear single quantum coherence
FRET	fluorescence energy transfer

Introduction

The history of paramagnetic relaxation enhancement (PRE) and the nuclear Overhauser effect (NOE) dates back to the 1950s [1]. The NOE delineates short interproton distance contacts ($\leq 6\,\text{Å}$) and provides the main source of geometric information currently used in macromolecular NMR structure determination [2,3]. The PRE arises from magnetic dipolar interactions between a nucleus (e.g. ^{1}H) and the unpaired electrons of a paramagnetic center, and results in an increase in the relaxation rate of the nuclear magnetization [4]. For an electron–nucleus distance r, the magnitude of the PRE is proportional to r^{-6}, a relationship analogous to that between the magnitude of the NOE and interproton distance. However, because the magnetic moment of the unpaired electron is large, the PRE effects are large and can provide long-range distance information, extending in the case of Mn^{2+}, for example, up to $\sim 35\,\text{Å}$.

Not surprisingly, the PRE has seen extensive use in metalloproteins that possess a rigid intrinsic paramagnetic center [5–7]. Other systems necessitate the attachment of an extrinsic paramagnetic group to the macromolecule of interest through appropriate chemical modification. As a result, it is only relatively recently, with advances in biochemical methodology that permit the reliable conjugation of a paramagnetic group to a specific site, that the use of the PRE has seen a resurgence. The potential of the PRE for protein structure determination, however, was first demonstrated about 20 years ago on spin-labeled lysozyme and bovine pancreatic trypsin inhibitor [8,9].

Nitroxide spin labels or EDTA-Mn^{2+}, which have an unpaired electron with an isotropic g-tensor, are particularly suited for PRE measurements since they do not give rise to pseudo-contact shifts and Curie-spin relaxation is negligible. Recent applications include rapid determination of protein folds [10–15], analysis of unfolded and partially unfolded states [16,17••,18••,19•,20•], elucidation of protein-protein [21–24], protein-oligosaccharide [25,26,27••] and protein-nucleic acid [28–32] complexes, and studies of membrane protein structure [33•,34•]. Perhaps the most intriguing new application of the PRE relates to the study of low population encounter complexes involved in protein–nucleic acid [35••] and protein–protein [36,37••,38••] recognition, as well as the study of large-scale dynamics that entail significant changes in paramagnetic center–^{1}H distances, including, for example, nonspecific protein–DNA interactions [39,40••] and large-scale domain motions [41••].

Measurement of the PRE

The PRE rate, Γ, is simply given by the difference in relaxation rates measured in the paramagnetic and control diamagnetic states. In general, we feel that the transverse

PRE (Γ_2) is the most reliable way to make use of the PRE for two reasons [42••]. First, the large magnitude of the ^{1}H-Γ_2 PRE makes it a highly sensitive probe. This is because of the large nuclear gyromagnetic ratio of the proton and the primary dependence of ^{1}H-Γ_2 on the spectral density function at zero-frequency. Second, the transverse ^{1}H-Γ_2 rate is much less susceptible to internal motions and cross-relaxation than the longitudinal PRE rate, ^{1}H-Γ_1.

Quantitative application of the PRE requires that ^{1}H-Γ_2 rates be measured precisely and accurately. The majority of examples in the literature make use of a single time-point measurement in which two regular HSQC correlation spectra, one of the paramagnetic state, and the other of the diamagnetic state at the same concentration, are used to determine ^{1}H-Γ_2 rates from the equation $I_{\text{para}}(0)/I_{\text{dia}}(0) = R_{2,\text{dia}}\, e^{-\Gamma_2\tau}/(R_{2,\text{dia}} + \Gamma_2)$, where $I_{\text{para}}(0)$ and $I_{\text{dia}}(0)$ are the peak intensities in the paramagnetic and diamagnetic states, respectively, $R_{2,\text{dia}}$

is the transverse relaxation rate in the diamagnetic state, and τ is the overall ^{1}H transverse period for coherence transfers [42••]. Unfortunately, this simplistic approach severely underestimates the true value of ^{1}H-Γ_2 unless a very long repetition delay is employed (>20 s for a ^{2}H-labeled protein). This is because at short repetition delays, the recovery levels for the paramagnetic sample are always higher than those of the corresponding diamagnetic sample owing to the PRE on longitudinal relaxation rates (Γ_1). Accurate ^{1}H-Γ_2 rates, however, can be obtained in the same measurement time from a two time-point measurement without requiring any fitting procedures or complicated error estimations. ^{1}H-Γ_2 for the two time-point measurement is given by [31,42••]:

$$\Gamma_2 = R_{2,\text{para}} - R_{2,\text{dia}} = \frac{1}{T_{\text{b}} - T_{\text{a}}} \ln \frac{I_{\text{dia}}(T_{\text{b}})I_{\text{para}}(T_{\text{a}})}{I_{\text{dia}}(T_{\text{a}})I_{\text{para}}(T_{\text{b}})} \quad (1)$$

with errors in Γ_2 given by

Figure 1
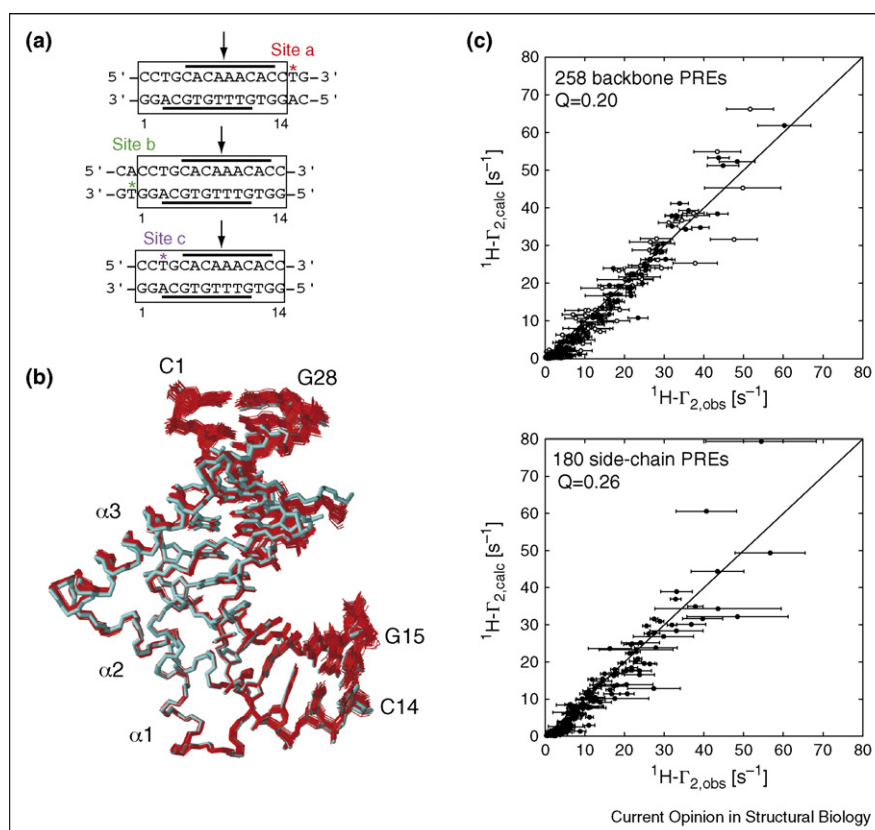
The intermolecular PRE in structure refinement of the SRY/DNA complex. **(a)** Oligonucleotides with location of the paramagnetic center (dT-EDTA-Mn^{2+}) indicated by an asterisk and color-coded. The location of the specific SRY binding site is indicated by the solid bars and the site of intercalation of Ile13 is shown by an arrow. **(b)** Best-fit superposition of 40 simulated annealing structures (red) refined against 438 intermolecular ^{1}H-PRE restraints (31) on the restrained regularized mean coordinates (cyan) generated from structures based on NOE, dipolar coupling, J coupling and torsion angle restraints calculated without ^{1}H-PRE restraints [58]. **(c)** Agreement between observed and calculated values of ^{1}H-Γ_2 rates for backbone and side-chain ^{1}H-PREs after refinement using a three-conformer ensemble representation for each paramagnetic center. Adapted from Ref. [31].

$$\sigma(\Gamma_2) = \frac{1}{T_b - T_a} \sqrt{\left\{\frac{\sigma_{dia}}{I_{dia}(T_a)}\right\}^2 + \left\{\frac{\sigma_{dia}}{I_{dia}(T_b)}\right\}^2 + \left\{\frac{\sigma_{para}}{I_{para}(T_a)}\right\}^2 + \left\{\frac{\sigma_{para}}{I_{para}(T_b)}\right\}^2} \qquad (2)$$

where T_a and T_b are the two time points, and σ_{para} and σ_{dia} are the standard deviations of the noise in the spectra recorded for the paramagnetic and diamagnetic states, respectively. By using a relatively short time interval for the two time-point measurement, errors in Γ_2 introduced by any potential diamagnetic contamination can also be significantly reduced [42••].

Using the PRE for structure determination

One of the most difficult aspects of using NOEs for protein structure determination relates to unambiguous crosspeak assignment [2,3]. Owing to extensive spectral overlap, it is often difficult to unambiguously assign a NOE crosspeak to a single interaction, even in four-dimensional spectra. Consequently, the strategy for structure determination generally relies on an iterative strategy in which a low-resolution fold is calculated on the basis of relatively few unambiguous NOE crosspeaks, followed by iterative refi-nement to assign all the remaining crosspeaks in the NOE spectra [3]. Not surprisingly, it is quite easy to make mistakes (i.e. proceed down an incorrect path), whether this process is carried out manually or automatically by computer algorithms [43]. The identification of a PRE effect, just like a residual dipolar coupling, on the other hand, is entirely straightforward, since the assignment of crosspeaks in the correlation

spectra are already known from through-bond scalar triple resonance experiments.

One of the intrinsic problems in making use of the PRE for structure determination is the fact that extrinsic paramagnetic probes are invariably conjugated to the macromolecule of interest via a flexible linker with several rotatable bonds. Thus, it is absolutely essential to treat the paramagnetic center by a multiple conformer representation [31]. If only a single conformer representation is employed, it may still be possible to fit the PRE data but at the expense of coordinate accuracy; that is to say inappropriate treatment of the PRE data will actually result in structural distortion and reduced coordinate accuracy [31]. Generally, a three-member ensemble for the paramagnetic center is sufficient, but in some cases a larger ensemble may be required. For a N-site jump model with appropriate ensemble averaging for the PRE, Γ_2, using a model-free extension of the Solomon–Bloembergen equations, is given by [31]:

$$\Gamma_2 = S_{PRE}^2 \langle r^{-6} \rangle f_{SB,2}(\tau_c) + (1 - S_{PRE}^2) \langle r^{-6} \rangle f_{SB,2}(\tau_t) \quad (3)$$

where τ_c is the correlation time defined as $(\tau_r^{-1} + \tau_s^{-1})^{-1}$ and τ_t is the total correlation time defined as

Figure 2
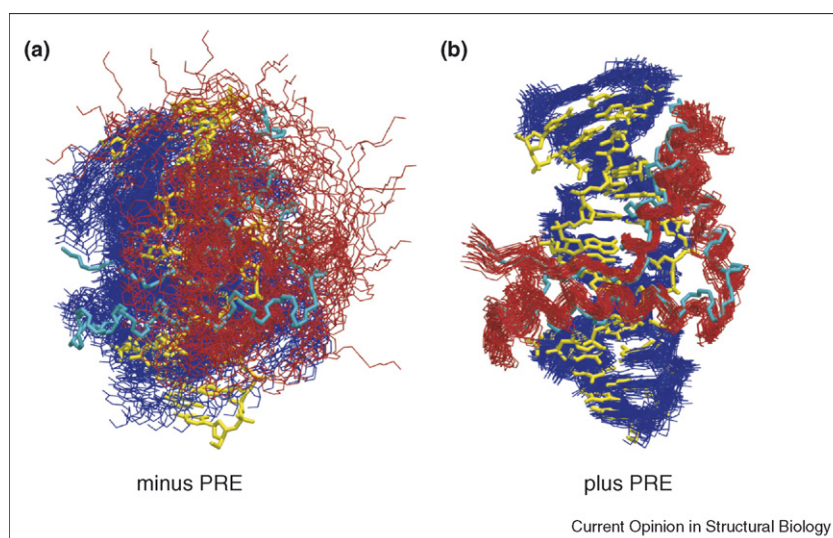
Impact of intermolecular PRE on coordinate accuracy of the SRY/DNA complex when only a single intermolecular NOE restraint located at the center of the protein–DNA interface is employed. Best-fit superposition of 30 simulated annealing structures (SRY, red, DNA, blue) calculated **(a)** without and **(b)** with 438 intermolecular ^{1}H-PRE restraints. The original restrained regularized mean structure of the SRY/DNA complex [58] determined using 168 intermolecular NOE restraints and 375 residual dipolar couplings is shown in cyan (SRY) and yellow (DNA). Adapted from Ref. [31].

Figure 3
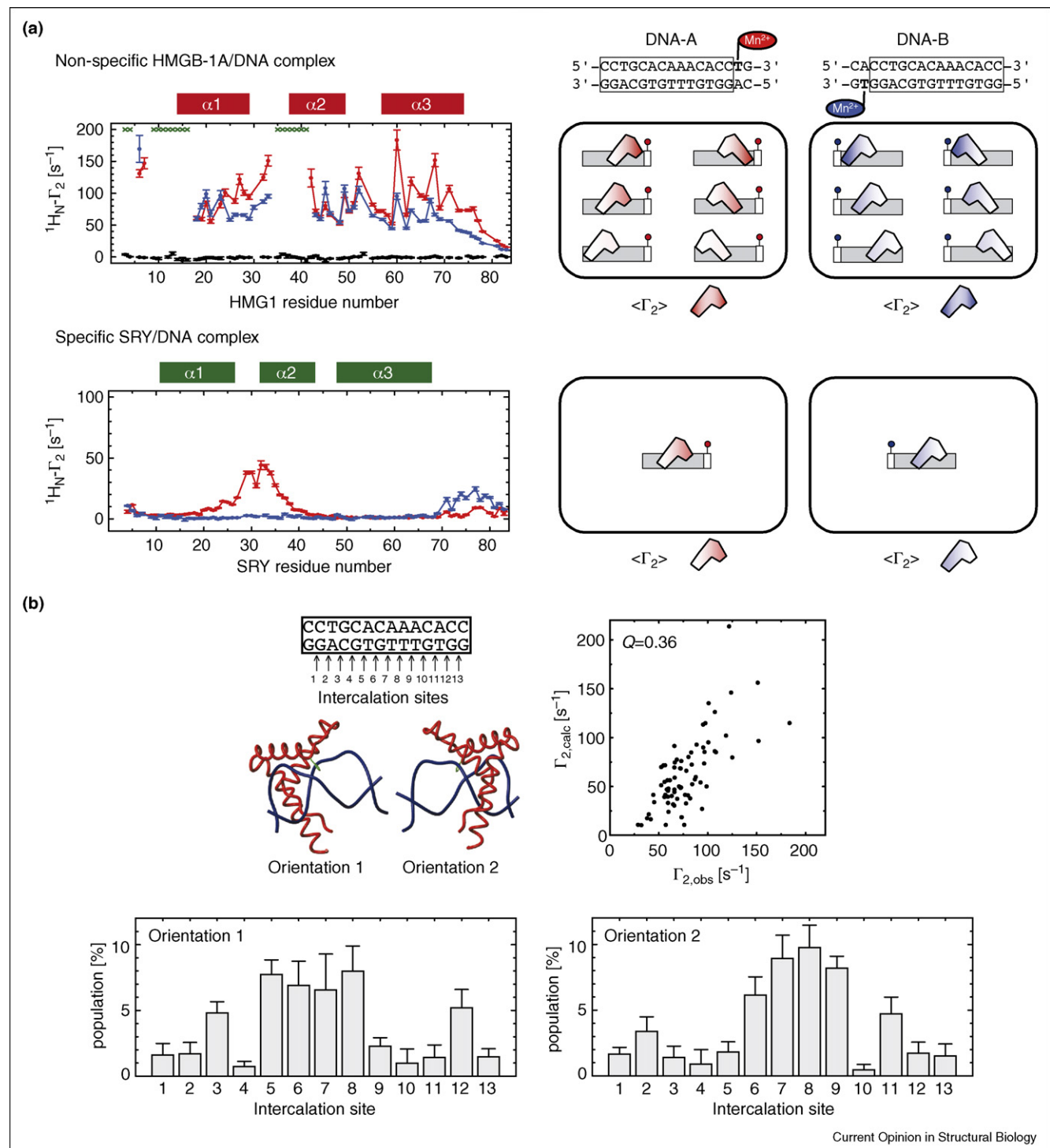
Characterization of nonspecific DNA binding of HMGB-1A by PRE. **(a)** Comparison of PRE profiles observed for the nonspecific HMGB-1A/DNA complex and the specific SRY/DNA complex with two DNA duplexes bearing dT-EDTA-Mn^{2+} at opposite ends of the DNA. A diagrammatic depiction of the states giving rise to the observed PREs is shown on the right-hand side of the figure. **(b)** Semi-quantitative estimation of the distribution and occupancy of HMGB-1A-binding sites along a 14-bp duplex DNA. There are 13 potential intercalation sites and HMGB-1A can bind in two orientations related by a 180° rotation (top left panel). The optimized distribution for the two orientations (bottom two panels) yields a PRE Q-factor of 0.36 (top right panel). Adapted from Ref. [39].

$(\tau_{\mathrm{r}}^{-1} + \tau_{\mathrm{s}}^{-1} + \tau_{\mathrm{i}}^{-1})^{-1}$. τ_{r}, τ_{s} and τ_{i} are the rotational correlation time, the effective electron relaxation time, and the internal correlation time, respectively. $r^{-6}f_{\mathrm{SB,2}}(\tau_{\mathrm{c}})$ corresponds to the classical Solomon–Bloembergen equation for Γ_2 [31]. $\langle r^{-6} \rangle$ is calculated as

$$\langle r^{-6} \rangle = \frac{1}{Nn_{\mathrm{p}}} \sum_{h}^{N} \sum_{s}^{n_{\mathrm{p}}} r_{\mathrm{hs}}^{-6} \quad (4)$$

where N is the ensemble size and n_{p} is the number of equivalent protons. The PRE order parameter S_{PRE}^2 is given by the product of angular and radial components:

$$S_{\mathrm{PRE}}^2 \approx S_{\mathrm{PRE,angular}}^2 S_{\mathrm{PRE,radial}}^2 \quad (5)$$

where the angular and radial components are given by

$$S_{\mathrm{PRE,angular}}^2 = \frac{1}{N^2 n_{\mathrm{p}}^2} \sum_{h,k}^{N} \sum_{s,t}^{n_p} \left\{ \frac{3}{2} \left(\frac{\vec{r}_{\mathrm{hs}} \cdot \vec{r}_{kt}}{r_{\mathrm{hs}} r_{kt}} \right)^2 - \frac{1}{2} \right\} \quad (6)$$

$$S_{\mathrm{PRE,radial}}^2 = \frac{\left(\sum_{h}^{N} \sum_{s}^{n_{\mathrm{p}}} r_{\mathrm{hs}}^{-3} \right)^2}{Nn_{\mathrm{p}} \sum_{h}^{N} \sum_{s}^{n_{\mathrm{p}}} r_{\mathrm{hs}}^{-6}} \quad (7)$$

Optimization of the conformer representation for the paramagnetic center is readily achieved using simulated annealing in torsion angle space [31]. A quantitative measure of agreement between observed and calculated Γ_2 rates can be obtained by calculating a Q-factor given by [31]:

$$Q \sqrt{\frac{\sum_i \{\Gamma_2^{\mathrm{obs}}(i) - \Gamma_2^{\mathrm{cal}}(i)\}^2}{\sum_i \Gamma_2^{\mathrm{obs}}(i)^2}} \quad (8)$$

In the context of tight macromolecular complexes, the PRE provides a very powerful additional source of inter-molecular distance restraints containing both translational and orientational information. Figure 1 shows an example of the results of structure refinement incorporating inter-molecular PRE data for the SRY/DNA complex [31]. Using an ensemble size of $N = 3$ for each paramagnetic center, 438 intermolecular ^{1}H-Γ_2 restraints, derived from three complexes with dT-EDTA-Mn^{2+} incorporated at three different sites, are readily satisfied without impacting the agreement with other experimental restraints, including residual dipolar couplings. In addition, complete cross-validation was able to demonstrate that the incorporation of PRE restraints results in significant gains in coordinate accuracy. The power of the PRE for studying intermolecular complexes is illustrated in Figure 2, which compares an ensemble of structures for the SRY/DNA complex calculated on the basis of only a single intermolecular NOE restraint: with no PRE data the orientation of SRY relative to the DNA cannot be deter-

mined; addition of the intermolecular PRE data allows the structure to be resolved unambiguously [31].

## Intermolecular PRE and nonspecific protein–DNA interactions

Structural characterization of nonspecific protein–DNA interactions in a system where the protein is not constrained to a single location but can dynamically sample all possible binding sites on the DNA during the course of the measurement represents a challenging problem since the experimental observables represent ensemble averages of all the states present in solution [39,40$^{\bullet\bullet}$]. Figure 3a compares the PRE profiles observed for the specific SRY/DNA complex versus that for the nonspecific HMG-1A/DNA complex [39]. The two proteins are members of the HMG-box family, bind in the minor groove and bend the DNA. The PRE profile for the SRY/DNA complex is fully consistent with a single

Figure 4
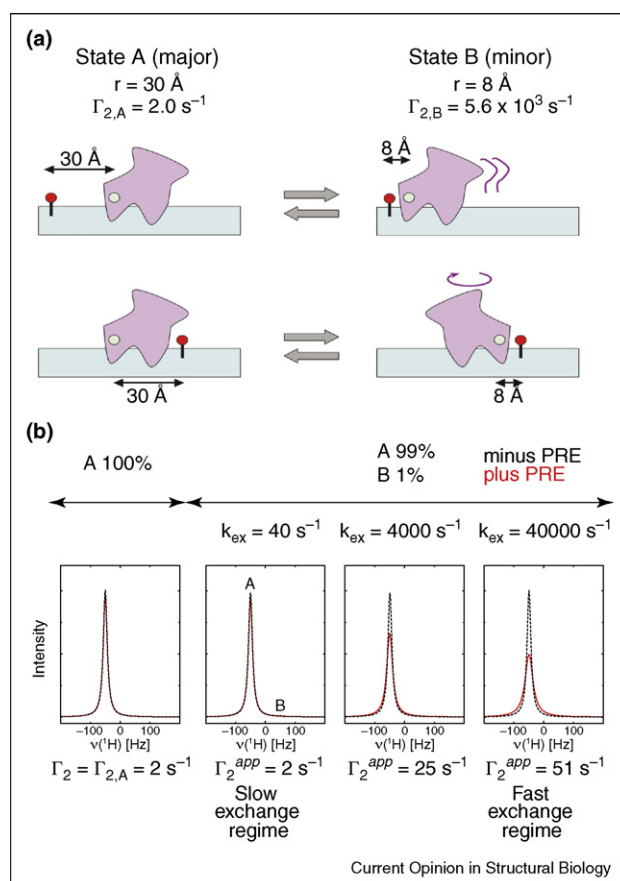
Intermolecular PRE in an exchanging system. **(a)** Diagrammatic depiction of a two site-exchange process involving major (99%) and minor (1%) species with paramagnetic-^{1}H distances of 30 and 8 Å, respectively. **(b)** Effect of increasing exchange rate on NMR line-shape with (red) and without (black) PRE. In the slow exchange regime the PRE is insensitive to presence of minor state; in the fast exchange regime, however, the PRE is sensitive to the presence of minor species and can be used to reveal the footprint of minor species. Adapted from Ref. [35$^{\bullet\bullet}$].

Figure 5
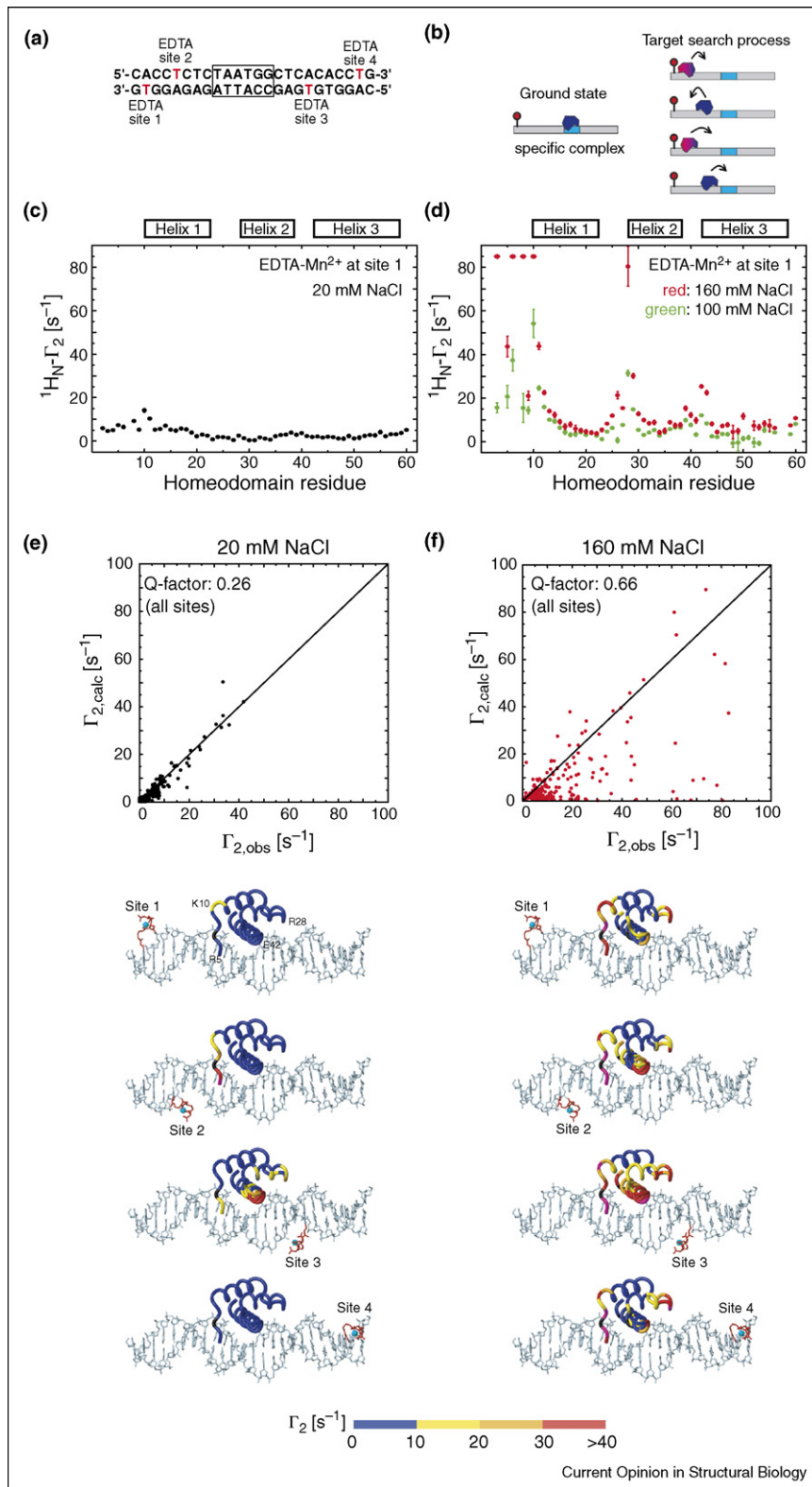
Intermolecular PREs observed for the HoxD9/DNA complex in the slow (20 mM NaCl) and fast (160 mM NaCl) exchange regimes. **(a)** DNA duplex containing the HoxD9 specific binding site (boxed) and showing the location of the four sites used to introduce dT-EDTA-Mn^{2+} (one at a time). **(b)** Schematic illustration of the ground state specific complex and the target search process. **(c)** and **(d)** PRE profiles observed for site 1 at low

specific complex (cf. Figure 1). For the HMG-1A/DNA complex, however, the PRE profiles observed with the dT-EDTA-Mn^{2+} paramagnetic center placed at either end of the DNA duplex are not only significantly larger than those observed for the specific SRY/DNA complex, but even more importantly are very similar to one another. The latter is diagnostic of multiple binding sites in multiple orientations. The former indicates the presence of binding sites close to the paramagnetic center, since Γ_2 is proportional to $\langle r_{Mn-H} \rangle^{-6}$ and hence strongly influenced by the minimum value of r_{Mn-H}. Similar results have been observed for nonspecific HoxD9 homeodomain/DNA complexes [40[••]].

It is possible to go one step further by carrying out a semi-quantitative analysis to ascertain the populations of individual binding states [39]. If we assume an N discrete binding state model where the transitions between the states are slower than the rotational correlation time but fast on the chemical shift time scale, the spectral density for a dipole–dipole interaction vector is independent of the transition rates and angles between the vectors of the individual states. The ensemble average $\langle \Gamma_2 \rangle$ rate is therefore given by the weighted average of the Γ_2 rates for the individual states [39]:

$$\langle \Gamma_2 \rangle = \sum_{k=1}^{N} \rho_k \Gamma_{2,k} \qquad (9)$$

where ρ_k and $\Gamma_{2,k}$ are the population and ^1H_N-Γ_2 PRE rate, respectively, for state k. The populations ρ_k can be obtained by back-calculating the Γ_2 rates from structural models of the individual states and minimizing the χ^2 function [39]:

$$\chi^2 = \sum_i \frac{\left\{ \Gamma_{2,\text{obs}}(i) - \sum_{k=1}^{N} \rho_k \Gamma_{2,\text{calc},k}(i) \right\}^2}{\sigma(i)^2} \qquad (10)$$

where i is the index for each data point; $\Gamma_{2,\text{obs}}(i)$ the observed value of ^1H-Γ_2; $\Gamma_{2,\text{calc},k}(i)$ the calculated value of ^1H-Γ_2 for binding state k; and $\sigma(i)$ the experimental error for $\Gamma_{2,\text{obs}}(i)$. The highest populations of binding are located around the central region of the DNA duplex, and the population in the two possible orientations is approximately equal (Figure 3b).

Using the PRE to study transient low-population intermediates in macromolecular interactions

In an exchanging system comprising two or more species in equilibrium, the observed PRE measured on the resonance of the major species will be modulated by the minor species, the extent of which depends upon the rate of exchange (k_{ex}) between the species [35[••]]. This phenomenon is most easily appreciated by considering a simple two-site exchange system in which the major species (A) has an occupancy of 99% with a paramagnetic center–proton distance of 30 Å, while the minor species (B, only 1%) has a paramagnetic center–proton distance of 8 Å (Figure 4). For a 30 kDa system, the ^1H-Γ_2 rate arising from Mn^{2+} will be $\sim$2 s^{-1} for the major species and $\sim$5600 s^{-1} for the minor one. When k_{ex} is slow ($<$50 s^{-1}), the presence of the minor species has no impact on the apparent Γ_2 rate (Γ_2^{app}) observed on the resonance of the major species. As k_{ex} increases, the apparent Γ_2 rate increases, when $k_{ex} \gg (\Gamma_2^B - \Gamma_2^A)$, Γ_2^{app} is given by the population weighted average of the Γ_2 rates of the two species. In this particular example, Γ_2^{app} will be $\sim$30 times larger than Γ_2^A, allowing one to both infer the presence of the minor species and derive structural information on it.

Intramolecular and intermolecular translocation in specific protein–DNA recognition

A long-standing question in protein–DNA recognition pertains to the search process whereby a transcription factor locates its specific cognate site among a sea of nonspecific sites. Both kinetic and theoretical considerations have suggested that nonspecific binding can significantly enhance the rate of specific recognition via two complementary mechanisms [44–47]: (a) intramolecular translocation or sliding that results in a reduction in the dimensionality of the search process from three dimensions to one and (b) intermolecular translocation or hopping from one DNA molecule to another or from one DNA segment to another via looping.

^{15}N z-exchange spectroscopy in which the HoxD9 homeodomain was mixed with an equimolar concentration of two DNA duplexes differing in only a single base pair mutation at the edge of the specific binding site demonstrated that intermolecular translocation occurs very efficiently at relatively high (submillimolar) DNA concentrations even at low salt (20 mM NaCl) [48[••]]. The apparent rate of this process is proportional to the concentration of free DNA, is highly dependent on salt concentration, and occurs via direct transfer without ever involving the intermediary of free protein [48[••]]. Given the extremely high concentration of DNA in the nucleus, intermolecular translocation represents an important pathway for the transfer of a transcription factor from one DNA site to another.

(Figure 5 Legend Continued) (20 mM NaCl) and high (100 and 160 mM NaCl) salt, respectively. (e) and (f) Correlation between observed and calculated PREs for all four sites at low (20 mM NaCl) and high (160 mM NaCl) salt, respectively. Below the correlation diagrams, the PRE data are mapped on the structural model of the HoxD9/DNA complex, with the color scale depicting Γ_2 rates. Adapted from Ref. [35[••]].

PRE measurements at low salt (20 mM NaCl) on the specific HoxD9/DNA complex are fully consistent with the crystal structure of the highly homologous *antennapedia* homeodomain/DNA complex [35••]. The overall PRE Q-factor (Q_{PRE}) for the data collected from four different locations of the paramagnetic center along the DNA was 0.26 (Figure 5). As the salt concentration is raised to 100 and 160 mM NaCl, however, the PRE data are completely inconsistent with the structure of the specific complex (Q_{PRE} = 0.66), and the profiles reflect the footprint of binding intermediates involved in the target search process (Figure 5), even though the value of K_{diss} is 1.5 nM at 100 mM NaCl. The observed PREs at high salt cannot be attributed to structural changes since the observed spectrum remains unaltered and the dipolar coupling data are fully consistent with the crystal structure [35••].

The observed PRE profiles on the specific HoxD9/DNA complex can be attributed to intramolecular and/or intermolecular translocation. To assess the relative contributions of these two processes, two experiments were carried out involving HoxD9 in the presence of equal

mixtures of two DNA duplexes (Figure 6): sample 1 comprised the specific duplex without a paramagnetic center and a nonspecific duplex bearing the dT-EDTA-Mn^{2+} paramagnetic center; sample 2 comprised the specific duplex with dT-EDTA-Mn^{2+} and a nonspecific duplex without a paramagnetic center [35••]. In sample 1, intermolecular PREs can only occur via a mechanism involving intermolecular translocation, while for sample 2 both intramolecular and intermolecular translocation can contribute to the observed PREs. The PRE profiles for the two samples are very similar, indicating that intermolecular translocation is a major contributor. Upon further examination of the PRE profiles, however, it is apparent that the Γ_2 rates for residues 24–33 and 41–42 are 30–100% larger for sample 2 than those for sample 1, whereas those for the N-terminal arm region are the same. The larger PRE values for a limited region of the protein in sample 2 are directly attributable to intramolecular translocation which gives rise to bias arising from the fact that the orientation of the protein bound to the specific site is favored as the protein slides along the DNA [35••]. Thus, as the protein slides away from the specific site, residues 24–33 and 41–42 can readily come into very close

Figure 6
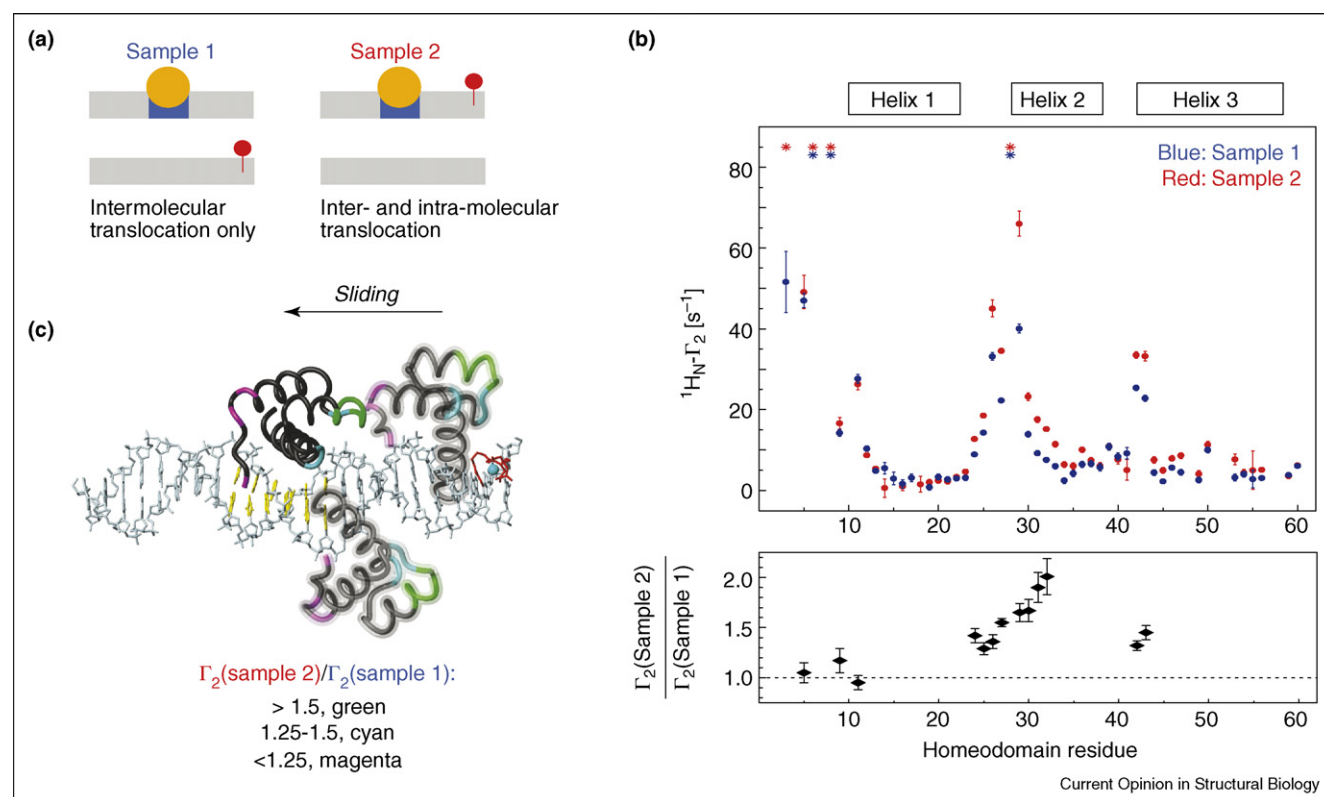
Intramolecular and intermolecular translocation in the HoxD9/DNA system. **(a)** PRE data were collected on HoxD9 in the presence of equal mixture of two DNA duplexes, one with and the other without the specific site (indicated in blue). In sample 1, the nonspecific DNA bears the paramagnetic center and PREs only arise from intermolecular translocation; in sample 2, the specific DNA has the paramagnetic center and PREs can arise from both intermolecular and intramolecular translocation. **(b)** Observed PRE profiles. **(c)** Schematic representation of sliding along the DNA with HoxD9 color coded according to the Γ_2(sample 2)/Γ_2(sample 1) ratio. Adapted from Ref. [35••].

proximity to the paramagnetic center; the N-terminal tail, however, can only approach the paramagnetic center following an intermolecular translocation event resulting in a 180° flip in the binding orientation of the protein along the DNA duplex.

Transient encounter complexes in protein–protein recognition

Kinetic studies on many protein–protein associations suggest the formation of a pre-equilibrium encounter complex that subsequently relaxes to the stereospecific complex. Further, site-specific mutagenesis studies and Brownian dynamics simulations have provided evidence of modulation of association rate constants via perturbations involving charged residues located outside the specific interaction surfaces [49–52]. This suggests that nonspecific encounter complexes may facilitate protein–protein recognition either by a reduction in dimensionality, in this instance from a three-dimensional to two-dimensional

search process [53], or by the presence of a short-range, nonspecific attractive potential [47]. We set out to detect such encounter complexes by means of PRE measurements using a relatively weak complex ($K_{diss} \sim 10~\mu M$) comprising the N-terminal domain of enzyme I (EIN) and HPr. The 40 kDa EIN/HPr complex had previously been solved by NMR on the basis of extensive NOE and dipolar coupling measurements [54]. This complex catalyzes the transfer of a phosphoryl group from His189 of EIN to His15 of HPr, and the NMR structure of the complex is fully consistent with the formation of a pentacoordinate phosphoryl transition state intermediate without requiring any significant structural perturbation [54]. EDTA-Mn^{2+} was introduced at three separate sites (E5C, E25C and E32C) on HPr, and intramolecular and intermolecular PRE data were measured [37[••]]. The intramolecular PRE data observed for HPr are fully consistent with the X-ray structure of HPr with an overall intramolecular PRE Q-factor of 0.18 (Figure 7a). Although the intermolecular

Figure 7
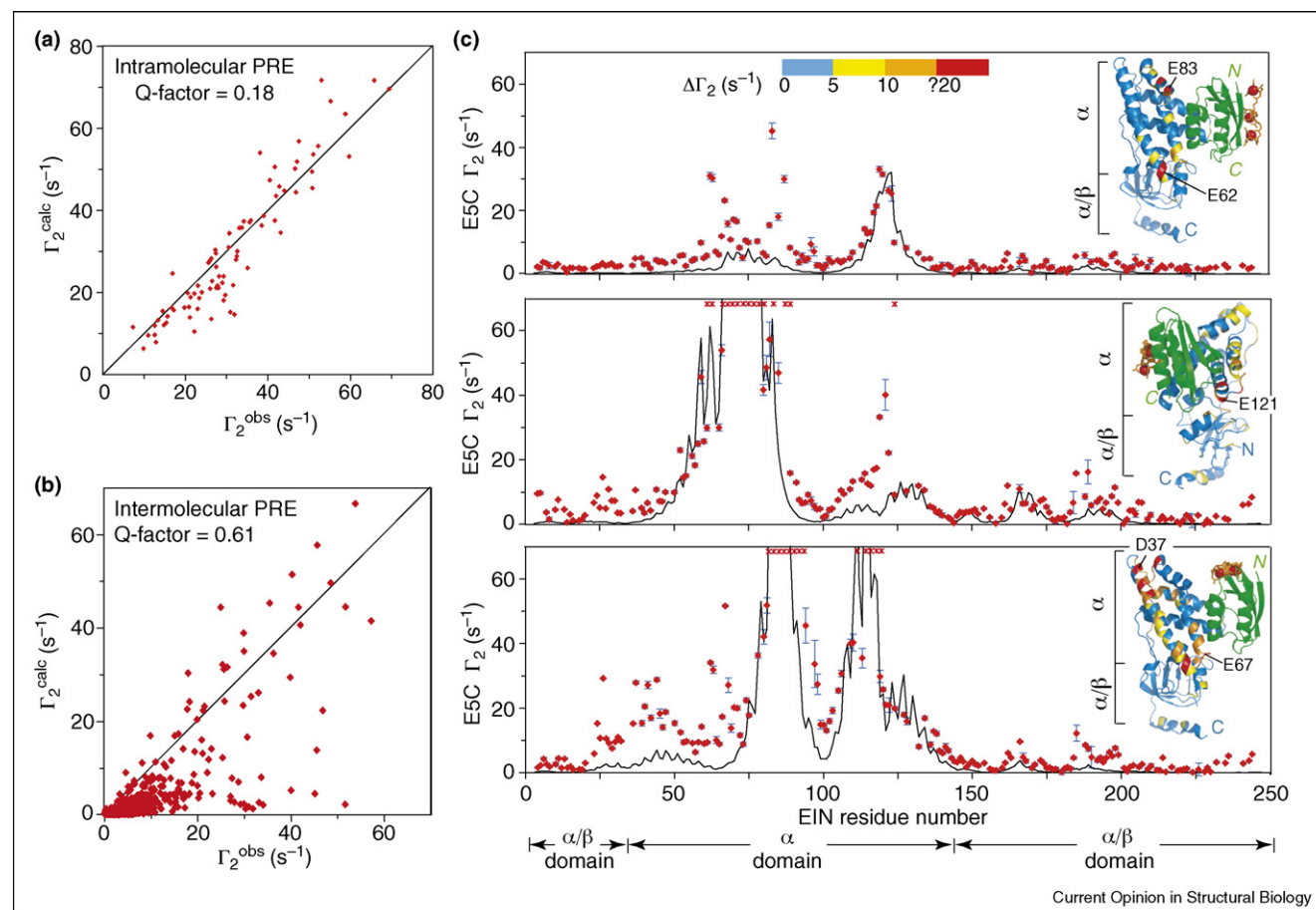
Intermolecular PREs for the EIN-HPr complex. EDTA-Mn^{2+} was conjugated to an engineered surface cysteine at three sites (E5C, E25C, and E32C). **(a)** Correlation between observed and calculated intramolecular Γ_2 rates for HPr. **(b)** Correlation between observed and calculated intermolecular Γ_2 rates measured on EIN and arising from paramagnetically labeled HPr. **(c)** Intermolecular PRE profiles observed for the three sites, with experimental Γ_2 rates denoted by the red circles, and the theoretical Γ_2 rates calculated from the structure of the stereospecific complex by the black line. Adapted from Ref. [37[••]].

PRE profiles observed on EIN display features that clearly arise from the stereospecific complex, other features are present indicative of the presence of alternative modes of binding involving nonspecific encounter complexes (Figure 7c). As a result the overall intermolecular PRE Q-factor calculated from the stereospecific complex is 0.61 and the correlation between observed and calculated Γ_2 rates is poor (Figure 7b).

A semi-quantitative description of the observed intermolecular PRE data for the EIN-HPr complex can be obtained by direct rigid body simulated annealing refinement [55] of a system comprising the stereospecific complex (whose structure is fixed) with population λ in rapid exchange with an ensemble of encounter complexes comprising N states with overall population $(1 - \lambda)$ (Figure 8) [37[••]]. Complete cross-validation indicates that the encounter complexes is best represented by an ensemble of size $N = 10–20$ at a population of $\sim$10%. The resulting intermolecular PRE Q-factor is 0.21. When the distribution of the nonspecific encounter complexes is examined, there appears to be a qualitative correlation with electrostatic potential, with the positively charged face of HPr populating regions of EIN with highly negative electrostatic potentials (Figure 9). Interestingly, the region occupied by the stereospecific complex is only minimally populated by nonspecific encounter complexes suggesting that once HPr reaches this region, formation of the stereospecific complex occurs with high probability [37[••]]. The characteristics of the nonspecific encounter complexes are quite distinct from the stereospecific complex that possesses a well-defined array of complementary van der Waals and electrostatic interactions [54]. The buried accessible surface area at the protein–protein interface is on average an order of magnitude smaller, the gap index is much larger (i.e. the interface is less well packed), and the interfacial composition of charged residues is increased for the nonspecific encounter complexes relative to the stereospecific complex [37[••]].

Figure 8
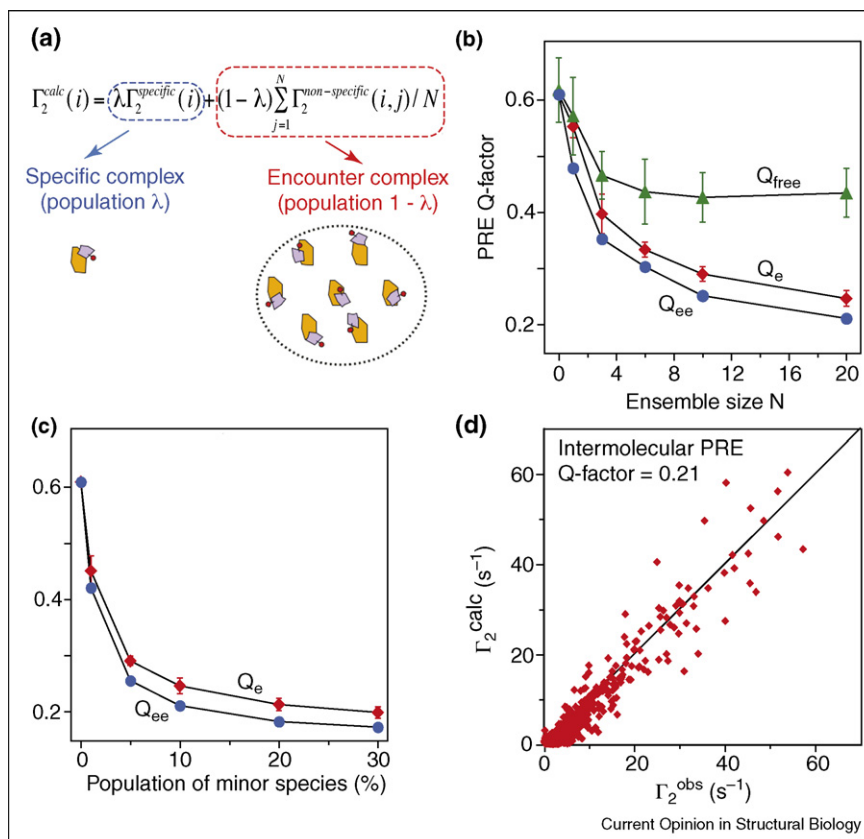
Ensemble refinement of intermolecular PRE data for the EIN-HPR complex. **(a)** The observed Γ_2 rates in the fast exchange regime are a weighted average of the Γ_2 rates for the specific complex and an encounter complex ensemble comprising N species. **(b)** Dependence of working (Q_e and Q_{ee}) and complete cross-validated (Q_{free}) Q-factors on ensemble size N. **(c)** Dependence of working Q factors on population of the encounter complex ensemble. **(d)** Correlation between observed and calculated Γ_2 rates obtained with a population of 10% for the encounter complex species represented by an ensemble of size $N = 20$. Q_e is the average Q-factor $\langle Q \rangle$ for all 100 calculated ensembles and Q_{ee} is the ensemble of ensembles average Q-factor. Adapted from Ref. [37[••]].

Figure 9

Current Opinion in Structural Biology
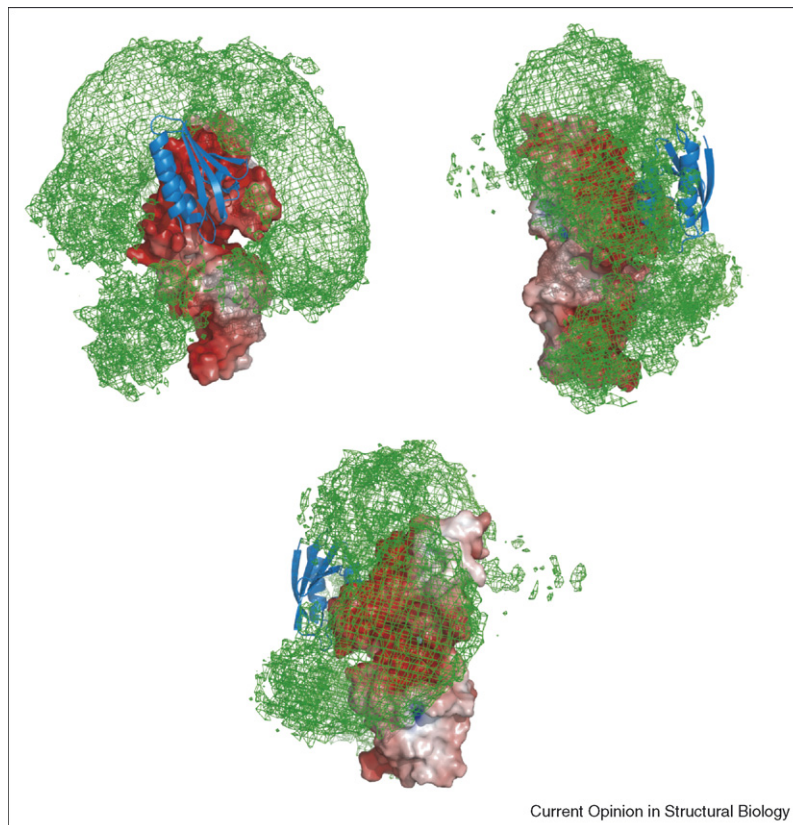
Three views of a reweighted atomic probability map illustrating the distribution of HPr molecules on the surface of EIN that make up the ensemble of encounter complexes. The encounter complex probability map (green mesh plotted at a threshold of 20% maximum) is calculated from 100 independent calculations of ensemble size $N = 20$ at a population of 10%; the molecular surface of EIN is color coded by electrostatic potential (± 8 kT); and the location of HPr in the stereospecific complex is shown as a blue ribbon. Adapted from Ref. [37••].

The direct detection of nonspecific encounter complexes by PRE is quite general for systems with relatively weak affinity. We observed similar phenomena for two other complexes involving HPr and the proteins IIA$^{\text{Mannitol}}$ and IIA$^{\text{Mannose}}$ [37••]. Contemporaneously, similar observations have been made for the interaction of cytochrome c and cytochrome c peroxidase [38••]. These findings probably reflect a general principle of steered macromolecular diffusion and protein–protein association whereby weak, transient, nonspecific encounter complexes are formed, presumably via long-range nonspecific electrostatic interactions supplemented by short-range van der Waals ones, thereby facilitating the rapid formation of the stereospecific complex [37••]. The nonspecific encounter complexes are sufficiently long-lived to permit a two-dimensional search on the surface of the proteins, until the region of the specific interaction surfaces is reached and the complex falls into a narrow energy funnel that leads rapidly and directly to the formation of the stereospecific complex. Very recently, using chemical shift mapping and NMR relaxation dispersion measurements, nonspecific encounter complex formation has also been

shown to play a key role in coupled folding and binding of an intrinsically disordered peptide to its target protein [56••].

Concluding remarks

The PRE provides a very powerful tool for studying both structure and large-scale dynamic phenomena in solution. In terms of structure, the PRE is particularly useful since Γ_2 rates are measured from through-bond correlation spectra and hence the effects can be unambiguously assigned to specific paramagnetic center–proton interactions with little effort. Unlike FRET measurements where only a single distance between two fluorescent labels can be measured from a single sample [57], the PRE affords the simultaneous measurements of hundreds of paramagnetic center–proton distances. For direct refinement against PRE data it is crucial that accurate Γ_2 rates be obtained and that the extrinsic paramagnetic center be represented by an ensemble. The application of the PRE for structure determination of complexes, however, must be restricted to systems in slow exchange, since the presence of transient intermediates in fast

exchange with the major species may significantly impact the observed PREs, particularly when the paramagnetic center–proton distances are shorter in the minor species than the major one. This is because of the fact that the magnitude of the PRE is proportional to $\langle r^{-6} \rangle$ and hence heavily weighted by shorter paramagnetic center–proton distances. Although this represents a caveat in the use of the PRE for structure determination of complexes, it affords a unique tool to easily detect, visualize and characterize transient, low population intermediates or species at equilibrium. Even if the population of the intermediate species is as low as 1%, the PRE permits structural information relating to such species to be obtained. The effect, of course, depends crucially on time scale and the intermediates can only be detected in the fast exchange regime. We foresee that the PRE will yield unique insights into large-scale domain motions, the recognition processes involved in macromolecular interactions, and the formation of higher order complexes.

Acknowledgements

References and recommended reading

Papers of particular interest, published within the annual period of review, have been highlighted as:

- of special interest
- •• of outstanding interest

1. Solomon I: **Relaxation processes in a system of two spins**. *Phys Rev* 1955, **99**:559-565.

2. Wüthrich K: **NMR of Proteins and Nucleic Acids**. New York: John Wiley; 1986.

3. Clore GM, Gronenborn AM: **Two, three and four dimensional NMR methods for obtaining larger and more precise three-dimensional structures of protein in solution**. *Ann Rev Biophys Biophys Chem* 1991, **20**:29-63.

4. Bloembergen N, Morgan LO: **Proton relaxation times in paramagnetic solutions: effects of electron spin relaxation**. *J Chem Phys* 1961, **34**:842-850.

5. Cheng H, Markley JL: **NMR spectroscopic of paramagnetic proteins: iron sulfur proteins**. *Ann Rev Biophys Biomol Struct* 1995, **24**:209-237.

6. Bertini I, Luchinat C, Licciolini M: **Paramagnetic probes in metalloproteins**. *Methods Enzymol* 2001, **339**:314-340.

7. Ubbink M, Worral JAR, Canters GW, Groenen EJJ, Huber M: **Paramagnetic resonance of biological metal centers**. *Ann Rev Biophys Biomolec Struct* 2002, **31**:393-422.

8. Schmidt PG, Kuntz ID: **Distance measurements in spin-labeled lyzozyme**. *Biochemistry* 1984, **23**:4261-4266.

9. Kosen PA, Scheek RM, Naderi H, Basus VJ, Manogaran S, Schmidt PG, Oppenheimer NJ, Kuntz ID: **Two-dimensional ¹H-NMR of three spin-labeled derivatives of bovine pancreatic trypsin inhibitor**. *Biochemistry* 1986, **25**:2356-2364.

10. Kosen PA: **Spin labeling of proteins**. *Methods Enzymol* 1989, **177**:86-121.

11. Battiste JL, Wagner G: **Utilization of site-directed spin-labeling and high-resolution heteronuclear nuclear magnetic resonance for global fold determination of large proteins with limited nuclear Overhauser effect data**. *Biochemistry* 2000, **39**:5355-5365.

12. Gaponenko V, Howarth JW, Columbus G, Gasmi-Seabrook J, Yuan WL, Hubbell PR, Rosevear PR: **Protein global fold determination using site-directed spin and isotope labeling**. *Protein Sci* 2000, **9**:302-309.

13. Donaldson LW, Skrynnikov WY, Choy DR, Muhandiram B, Sarkar JD, Forman-Kay JD, Kay LE: **Structural characterization of proteins with an attached ATCUN motif by paramagnetic relaxation enhancement NMR spectroscopy**. *J Am Chem Soc* 2001, **123**:9843-9847.

14. Dvotretzky A, Gaponenko V, Rosevear PR: **Derivation of structural restraints using a thiol-reactive chelator**. *FEBS Lett* 2002, **528**:189-192.

15. Pintacuda G, Mosref A, Leonchiks A, Shapiro A, Otting G: **Site-specific labeling with a metal chelator for protein structure refinement**. *J Biomol NMR* 2004, **29**:351-361.

16. Gillespie JR, Shortle D: **Characterization of long-range structure in the denatured state of staphylococcal nuclease. I. Paramagnetic relaxation enhancement by nitroxide spin labels**. *J Mol Biol* 1997, **268**:158-169.

17. Bertoncini CW, Jung YS, Fernandrez CO, Hoyer W, Griesinger C,
•• Jovin TM, Zweckstetter M: **Release of long-range tertiary interactions potentiates aggregation of natively unstructured α-synuclein**. *Proc Natl Acad Sci USA* 2005, **102**:1430-1435.
In this study, using both PRE and dipolar coupling measurements, the authors show that intrinsically disordered α-synuclein assumes transient conformations that are stabilized by long-range interactions and act to inhibit oligomerization and aggregation.

18. Dedmon MM, Lindorff-Larsen K, Chistodoulou J, Vendruscolo M,
•• Dobson CM: **Mapping long-range interactions in α-synuclein using spin-label NMR and ensemble molecular dynamics simulations**. *J Am Chem Soc* 2005, **127**:476-477.
In this study, using PRE measurements the authors show that α-synuclein adopts a broad distribution of conformations with an ensemble averaged hydrodynamic radius that is significantly smaller than that expected for a random coil.

19. Krisjansdottir S, Lindorff-Larsen K, Fieber W, Dobson CM,
• Vendruscolo M, Poulsen FM: **Formation of native and non-native interactions in ensembles of denatured ACBP molecules from paramagnetic relaxation enhancement studies**. *J Mol Biol* 2005, **347**:1053-1062.
In this study, the authors use the PRE to show that denatured acyl coenzyme A binding protein has some residual structure with long-range interactions present.

20. Vise P, Baral B, Stancik A, Lowry DF, Daughdrill GW: **Identifying
• long-range structure in the intrinsically unstructured transactivation domain of p53**. *Proteins: Struct Funct Bioinformatics* 2007, **67**:526-530.
In this study, the PRE is used to demonstrate the presence of long-range transient structure for the intrinsically disordered activation domain of p53.

21. Mahoney NM, Rastogi VK, Cahill SM, Girvin ME, Almo SC: **Binding orientation of proline-rich peptides in solution: polarity of the profilin-ligand interaction**. *J Am Chem Soc* 2000, **122**:7851-7852.

22. Mal TK, Ikura M, Kay LE: **The ATCUN domain as a probe of intermolecular interactions: application to calmodulin-peptide complexes**. *J Am Chem Soc* 2002, **124**:14002-14003.

23. Gross JD, Moerke NJ, van deer Haar R, Lugovsky AA, Sachs AB, McCarthy JE, Wagner G: **Ribosome loading onto the mRNA cap is driven by conformational coupling between eIF4G and eIF4E**. *Cell* 2003, **115**:739-750.

24. Card PB, Erbel PJA, Gardner KH: **Structural basis of ARNT PAS-B dimerization: use of a common β-sheet interface for hetero- and homodimerization**. *J Mol Biol* 2005, **353**:664-677.

25. Johnson PE, Brun E, MacKenzie LF, Withers SG, McIntosh LP: **The cellulose-binding domains from *Cellulomonas fimi* β-1,4-glucanase CenC bind nitroxide spin-labeled cellooligosaccharides in multiple orientations**. *J Mol Biol* 1999, **287**:609-625.

26. Jain NU, Venot K, Umemoto H, Leffler H, Prestegard JH: **Distance mapping of protein binding sites using spin-labeled oligosaccharide ligands**. *Protein Sci* 2001, **10**:2393-2400.

27. Macnaughtan MA, Kamar M, Alvarez-Manilla G, Venot A,
•• Glushka J, Pierce JM, Prestegard JH: **NMR structural characterization of substrates bound to N-acetylglucosaminyltransferase**. *J Mol Biol* 2007, **366**:1266-1281.
In this study, the authors make use of a novel PRE experiment arising from a spin-labeled analogue of one of the two ligands of the 95 kDa enzyme N-acetylglucosaminyltransferase V to elucidate the orientation of the bound donor and acceptor ligands.

28. Ramos A, Varani G: **A new method to detect long-range protein-RNA contacts; NMR detection of electron–proton relaxation induced by nitroxide spin-labeled RNA**. *J Am Chem Soc* 1998, **120**:10992-10993.

29. Varani L, Gundersdon IW, Mattaj IW, Kay LE, Neuhaus D, Varani G: **The NMR structure of the 38 kDa U1A protein-PIE RNA complex reveals the basis of cooperativity in regulation of polyadenylation by human U1A protein**. *Nat Struct Biol* 2000, **7**:329-335.

30. Iwahara J, Anderson DE, Murphy EC, Clore GM: **EDTA-derivatized deoxythymidine as a tool for rapid determination of protein binding polarity to DNA by intermolecular paramagnetic relaxation enhancement**. *J Am Chem Soc* 2003, **125**:6634-6635.

31. Iwahara J, Schwieters CD, Clore GM: **Ensemble approach for NMR structure refinement against ¹H paramagnetic relaxation enhancement data arising from flexible paramagnetic group attached to a macromolecule**. *J Am Chem Soc* 2004, **126**:5879-5896.

32. Ueda T, Kato A, Ogawa T, Torizawa T, Kuramitsu S, Iwai S, Terasawa H, Shimada I: **NMR study of repair mechanism of DNA photolyase by FAD-induced paramagnetic relaxation enhancement**. *J Biol Chem* 2004, **279**:52574-52579.

33. Roosild TP, Greenwald J, Vega S, Castronovo S, Riek R, Choe S:
• **NMR structure of Mistic, a membrane-integrating protein for membrane protein expression**. *Science* 2005, **307**:1317-1321.
In this study an example of the use of the PRE as an aid in structure determination of membrane bound proteins.

34. Liang B, Bushweller JH, Tamm LK: **Site-directed parallel spin-**
• **labeling and paramagnetic relaxation enhancement in structure determination of membrane proteins by solution NMR spectroscopy**. *J Am Chem Soc* 2006, **128**:4389-4397.
In this study a demonstration of the utility of the PRE arising from multiple spin-labeled sites to facilitate the structure determination of a membrane-bound protein for which traditional NOE data are sparse and difficult to obtain.

35. Iwahara J, Clore GM: **Detecting transient intermediates in**
•• **macromolecular binding by paramagnetic NMR**. *Nature* 2006, **440**:1227-1230.
PRE data collected on the HoxD9 homeodomain/DNA specific complex at moderate salt concentrations provides the first direct demonstration for the existence of transient intermediates formed in a stochastic manner at noncognate sites involving both intramolecular sliding of HoxD9 along the DNA and intermolecular hopping of HoxD9 from one DNA molecule to another.

36. Hansen DF, Hass MAS, Christensen HM, Ulstrup J, Led JJ: **Detection of short-lived transient protein-protein interactions by intermolecular nuclear paramagnetic relaxation: plastocyanin from Anabaena variabilis**. *J Am Chem Soc* 2003, **125**:6858-6859.

37. Tang C, Iwahara J, Clore GM: **Visualization of transient**
•• **encounter complexes in protein–protein association**. *Nature* 2006, **444**:383-386.
This paper illustrates the first quantitative demonstration of the use of the PRE to demonstrate the existence and visualize the distribution of an ensemble of transient nonspecific encounter complexes under equilibrium conditions in protein–protein association. The existence of such encounter complexes is demonstrated for three different protein–protein associations involving complexes from the bacterial phosphotransferase system.

38. Volkov AN, Worall JAR, Holtzmann H, Ubbink M: **Solution**
•• **structure and dynamics of the complex between cytochrome c**

and cytochrome c peroxidase determined by paramagnetic NMR. *Proc Natl Acad Sci USA* 2006, **103**:18945-18950.
In this study, the conformational space sampled by two electron transfer proteins before the formation of a stereospecific electron transfer complex is investigated using the PRE.

39. Iwahara J, Schwieters CD, Clore GM: **Characterization of nonspecific protein-DNA interactions by ¹H paramagnetic relaxation enhancement**. *J Am Chem Soc* 2004, **126**:12800-12808.

40. Iwahara J, Zweckstetter M, Clore GM: **NMR structural and**
•• **kinetic characterization of a homeodomain diffusing and hopping on non-specific DNA**. *Proc Nat Acad Sci USA* 2006, **103**:15062-15067.
This paper makes use of multiple NMR spectroscopic techniques to characterize the structural and kinetic features of a nonspecific protein–DNA complex in which the protein can both hop and slide on the DNA. The data demonstrate unambiguously that HoxD9 binds to nonspecific DNA with the same binding mode and orientation as that observed for the specific complex.

41. Baker KA, Hilty C, Peti W, prince A, Pfaffinger PJ, Wider K,
•• Wüthrich K, Choe S: **NMR-derived dynamic aspects of N-type inactivation of a Kv channel suggest a transient interaction with the T1 domain**. *Biochemistry* 2006, **45**:1663-1672.
In this study, PRE measurements are used to demonstrate that there exists a small population of conformers in which the N-terminal inactivation peptide of the voltage-gated K⁺ channel is in close proximity to the tetramerization domain, providing direct evidence for large-scale inter-domain motions.

42. Iwahara J, Tang C, Clore GM: **Practical aspects of ¹H transverse**
•• **paramagnetic relaxation enhancement measurements on macromolecules**. *J Magn Reson* 2007, **184**:185-195.
In this study, a detailed analysis of the practical aspects of PRE measurements is presented.

43. Kuszewski J, Schwieters CD, Garrett DS, Byrd RA, Tjandra N, Clore GM: **Completely automated, highly error tolerant macromolecular structure determination from multidimensional nuclear Overhauser enhancement spectra and chemical shift assignments**. *J Am Chem Soc* 2004, **126**:6258-6273.

44. Berg OG, von Hippel PH: **Diffusion-controlled macromolecular interactions**. *Ann Rev Biophys Biophys Chem* 1985, **14**:131-160.

45. von Hippel PH, Berg OG: **Facilitated target location in biological systems**. *J Biol Chem* 1989, **264**:675-678.

46. Halford SE, Marko JF: **How do site-specific DNA-binding proteins find their targets?** *Nucl Acids Res* 2004, **32**:3040-3052.

47. Zhou HX, Szabo A: **Enhancement of association rates by non-specific binding to DNA and cell membranes**. *Phys Rev Lett* 2004, **204(93)**:101-178.

48. Iwahara J, Clore GM: **Direct observation of enhanced**
•• **translocation of a homeodomain between DNA cognates sites by NMR exchange spectroscopy**. *J Am Chem Soc* 2006, **128**:404-405.
In this study, a novel approach is described to analyze the kinetics of specific protein–DNA interactions using z-exchange spectroscopy on a system in which the DNA-binding protein is mixed with equimolar amounts of two DNA duplexes differing by a single base pair mutation at the edge of the DNA recognition site thereby producing slightly different chemical shifts for the two complexes without perturbing the equilibrium dissociation constant. Rapid direct hopping of HoxD9 from one DNA molecule to another without going through the intermediary of free protein is demonstrated with translocation rates that are over three orders of magnitude faster than the dissociation rate constant determined from gel shift assays at very low concentrations of free DNA.

49. Schreiber G, Fersht AR: **Rapid electrostatically assisted association of proteins**. *Nat Struct Biol* 1996, **3**:427-431.

50. Selzer T, Albeck S, Schreiber G: **Rational design of faster associating and tighter binding complexes**. *Nat Struct Biol* 2000, **7**:537-541.

51. Northrup SH, Boles JO, Reynolds JCL: **Brownian dynamics of cytochrome c and cytochrome c peroxidase association**. *Science* 1988, **241**:67-70.

52. Spaar A, Dammer C, Gabdoulline RR, Wade RC, Helms V:
     Diffusional encounter of barnase and barstar. *Biophys J* 2006,
     90:1913-1924.

53. Adams G, Delbruck M: **Reduction of dimensionality in biological
     diffusion processes**. In *Structural Chemistry and Molecular
     Biology.* Edited by Rich A, Davdison N. San Francisco: Freeman &
     Co.; 1968:198-215.

54. Garrett DS, Seok YJ, Peterkofsky A, Gronenborn AM, Clore GM:
     **Solution structure of the 40,000 M_r phosphoryl transfer
     complex between the N-terminal domain of enzyme I and HPr**.
     Nat Struct Biol 1999, **6**:166-173.

55. Schwieters CD, Kuszewski J, Clore GM: **Using Xplor-NIH for
     NMR molecular structure determination**. *Progr Nucl Magn
     Reson Spectrosc* 2006, **38**:47-62.

56. Sugase K, Dyson JH, Wright PE: **Mechanism of coupled folding
••   and binding of an intrinsically disordered peptide**. *Nature* 2007.
     Advance online publication doi:10.1038/nature05860.
     In this study, using chemical shift mapping and NMR relaxation disper-
     sion analysis the authors show that nonspecific encounter complexes are
     formed during the course of coupled folding and binding of an intrinsically
     disordered peptide to its target protein.

57. Hillisch A, Lorenz M, Diekman S: **Recent advances in FRET:
     distance determination in protein–DNA complexes**. *Curr Opin
     Struct Biol* 2001, **11**:201-207.

58. Murphy EC, Zhurkin VB, Louis JM, Cornilescu G, Clore GM:
     **Structural basis for SRY-dependent 46-X,Y sex reversal:
     modulation of DNA bending by a naturally occuring point
     mutation**. *J Mol Biol* 2001, **312**:481-499.